

Article

Effect of Coarse Aggregate and Multi-Wall Carbon Nanotubes on Heat Generation of Concrete

Hyojeong Yun ¹, Donghwi Kim ¹, Sunho Kang ² and Wonseok Chung ^{1,*} 

¹ Department of Civil Engineering, Kyung Hee University, 1732 Deokyoung-Daero, Giheung-gu, Yongin-si 17104, Gyeonggi-do, Republic of Korea; yunhj1201@khu.ac.kr (H.Y.); 0727donghwi@gmail.com (D.K.)

² Department of Civil Engineering, Chosun University, 309 Pilmun-Daero, Dong-gu, Gwangju 61452, Republic of Korea; lineho@chosun.ac.kr

* Correspondence: wschung@khu.ac.kr; Tel.: +82-31-201-2550; Fax: +82-31-202-8854

Abstract: Many researchers are developing heating construction materials to remove black ice from roads, addressing the scientific challenges associated with this issue. The use of carbon-based nanomaterials in concrete is of great interest due to the excellent electrical and thermal conductivity of this material. In this study, the incorporation of multi-walled carbon nanotubes (MWCNTs) into concrete compositions results in the formation of MWCNT bridge networks. MWCNTs exhibit a low specific heat and possess the ability to promptly generate raised temperatures with minimal power input. This characteristic has the potential to induce temperature variations in concrete. The heat generation test parameters for MWCNT concrete included the mixing concentration of the MWCNTs, the mixing ratio of coarse aggregate, the water/cement (W/C) ratio, and the presence or absence of superplasticizers. The heating performance of concrete was found to improve as the mixing concentration of the MWCNTs increased, while a heating performance decrease was observed as the mixing ratio of coarse aggregate increased, owing to the reduced dispersibility of the MWCNTs. Conversely, the heating performance improved when the W/C ratio increased due to the enhanced dispersibility of the MWCNTs. Moreover, superplasticizers assist in dispersing MWCNTs, thereby improving the heating performance. Additionally, field emission scanning electron microscopy revealed that MWCNTs form a bridge network between the cement hydrates. As a result of this study, the maximum temperature variation of concrete mixed with MWCNTs was up to 73.6 °C. Therefore, by mixing MWCNT aqueous solutions with concrete and using an appropriate W/C ratio and superplasticizer, a new construction material capable of enhanced heating performance was developed.

Keywords: multi-walled carbon nanotube; concrete; aggregate; heating performance



Citation: Yun, H.; Kim, D.; Kang, S.; Chung, W. Effect of Coarse Aggregate and Multi-Wall Carbon Nanotubes on Heat Generation of Concrete.

Buildings **2023**, *13*, 3127. <https://doi.org/10.3390/buildings13123127>

Academic Editors: Ramadhansyah Putra Jaya and Chuang Feng

Received: 14 November 2023

Revised: 14 December 2023

Accepted: 15 December 2023

Published: 17 December 2023



Copyright: © 2023 by the authors. Licensee MDPI, Basel, Switzerland. This article is an open access article distributed under the terms and conditions of the Creative Commons Attribution (CC BY) license (<https://creativecommons.org/licenses/by/4.0/>).

1. Introduction

Black ice is formed when water or snow seeps into small crevices present on the surface of asphalt or concrete and freezes. As the ice is thin and difficult to detect visually, black ice is a major contributing factor to traffic accidents. Given that sub-zero temperatures lead to the formation of black ice despite the application of snow-melting agents, it is essential to implement preventive snow-melting measures rather relying solely on reactive approaches. Typical preventive snow-melting solutions employ methods including the embedding of heating cables and thermal piping. Such methods excel in converting electricity or other energy sources into heat energy. However, frequent reinstallations are required due to the breakage of the heating cables or pipes under vehicle loading, thereby increasing maintenance costs. Hence, self-heating construction materials that avoid these drawbacks have been investigated. These materials are made conductive by introducing nanotechnology to conventional materials. Multi-walled carbon nanotubes (MWCNTs) stand as one of the commonly favored nanomaterials in the exploration of self-heating construction materials, primarily due to their thermal and electrical conductivities being 7.5 and 100 times higher,

respectively, than those of copper. Research into construction materials incorporating MWCNTs, known for these elevated thermal and electrical conductivities, is specifically directed towards enhancing their electrical conductivity and heating performance.

Li et al. [1] conducted a study on the snow-melting process using a cement composite containing MWCNTs. These experiments took place inside a freezer with external temperature conditions set at -30 , -20 , and -10 °C. The results revealed that as the outdoor temperature decreased, the time needed to melt the snow increased.

Gomis et al. [2] examined the heating performance of cement composites comprising carbon-based nanomaterials, for different types and concentrations of the parameters under investigation. The results indicated that the specimen with a 5 wt.% carbon nanotube (CNT) concentration experienced a maximum temperature change of approximately 65 °C within approximately 33 min. Kim et al. [3] explored the thermal and electrical properties of cement composites mixed with CNTs. Focusing on the concentration of CNTs, test specimens were prepared with 0.1, 0.3, 0.6, 1.0, and 2.0 wt.% of CNTs relative to the weight of cement. The heating performances of the cement composites were revealed to have improved as the incorporated CNT concentrations increased. The temperature of the specimen with a 2.0 wt.% CNT concentration peaked at approximately 67.8 °C. Further, Kim et al. [4] investigated the heating performance of cement composites mixed with CNTs by focusing on the applied power. The dimensions of the test specimens were 25 mm × 25 mm × 25 mm, with the CNT concentration fixed at 0.6 wt.% relative to the weight of the cement. The generated heat was found to be negligible for a power of 0–1 W but reached approximately 95 °C when 5 W or more was applied. Additionally, the heating performance increased linearly with the applied voltage. Lee et al. [5] conducted experiments on the heating performance of cement composites based on the type of CNTs used, including MWCNTs and single-walled carbon nanotubes (SWCNTs). SWCNTs improved the heating performance of the cement composite better than MWCNTs. Lee et al. [6] produced MWCNT-mixed cement composites and investigated their electrical and thermal characteristics by focusing on the concentration and method of MWCNT mixing. The mixing methods included dispersing MWCNTs in an aqueous solution and coating it on fine aggregate. The test specimens were produced with 0.125 and 0.25 wt.% of MWCNTs relative to the weight of cement, with the applied voltage set to 50 and 100 V. The MWCNT coating on fine aggregate produced a better heating performance than that of MWCNTs dispersed in an aqueous solution. Furthermore, Lee et al. [7] evaluated the heating performance of MWCNT-mixed cementitious composites at sub-zero temperatures by analyzing the mixing concentration of MWCNTs. The heating performances by the cementitious composites mixed with 1.0 wt.% MWCNTs increased by 51.4 times compared to those of specimens mixed with 0.1 wt.% MWCNTs. Additionally, the temperature of the cementitious composites mixed with 1.0 wt.% MWCNTs increased to approximately 21.7 °C at an outside temperature of -30 °C. Furthermore, methods for dispersing CNTs and addressing the uniformity issue during the cement-mixing process have been addressed through numerous studies [8–12].

Studies have also been conducted on concrete with coarse aggregate added to cement to improve the heating performance [1,3,13–15]. Won et al. [16] analyzed the thermal properties of a conductive heating pavement system capable of snow melting and de-icing. The conductive heating pavement system comprised a base concrete layer containing copper plates, a conductive cement composite layer, and a protective concrete layer. The conductive cement composite contained 5 wt.% graphite relative to the weight of the cement. The study confirmed a uniform temperature distribution with distances between the copper plates of 1000 and 1250 mm. Sassani et al. [17] developed electrically conductive concrete (ECON) on the runway of Des Moines Airport and conducted field tests to analyze its snow-melting performance. The results indicated that the optimal point for snow-melting performance was at a depth of 3 cm from the center of the slab. Using thermal imaging, it was confirmed that the ECON slab maintained its overall temperature, even when the outside temperature was -4.2 °C.

Cement mortar mixed with CNTs is being explored in various directions in research [18–22]. In addition to the heating performance, previous studies have focused on the electrical performance of cement mortar mixed with CNTs. Han et al. [23] explored MWCNT-mixed cement composites capable of self-sensing. The dimensions of the test specimens were 5.08 cm × 5.08 cm × 5.08 cm, and the electrical resistance was analyzed while applying compressive loads to the test specimens. The electrical resistances of the test specimens were found to decrease or increase when a load was applied or removed, respectively. In another study, Han et al. [24] investigated how the piezoresistivity of MWCNT-mixed cement composites is influenced by the concentration of MWCNTs and the water-to-cement (W/C) ratio. In this study, it was observed that the piezoresistivity initially increased with the mixing concentration of MWCNTs before eventually decreasing. Jang et al. [25] conducted experiments to analyze the electrical conductivity of CNT cementitious composites for different CNT mixing concentrations and moisture contents. The study demonstrated a sharp decline in the electrical conductivity of the CNT cementitious composite with a decrease in moisture, which was then improved with an increase in the CNT mixing concentration. Park et al. [26] investigated the electrical resistivity of cement composites mixed with pitch-based carbon fibers and CNTs, for different lengths and contents of the carbon fibers. The electrical resistances of the cement composite mixed with both pitch-based carbon fibers and CNTs and those mixed only with CNTs were found to be similar. The viscosity of the composite mixed with both pitch-based carbon fibers and CNTs improved by 90% compared to that with only CNTs, showing superior workability.

Most previous studies on construction materials mixed with MWCNTs have primarily focused on cement mortar or cement paste. However, MWCNT particles can agglomerate due to the van der Waals force between the particles, and, therefore, research on the heating characteristics of concrete mixed with MWCNTs is still limited. Concrete is more commonly used than cement mortar in most construction sites; therefore, research on its heating performance is essential. The composition of concrete varies depending on its intended use and strength requirements. The factors that can be changed during concrete fabrication include the aggregate ratio, W/C ratio, and the use of admixtures. The aggregate ratio and W/C ratio are closely related to the concrete strength, while superplasticizers are typical admixtures that reduce the unit water content of concrete. The workability of concrete can be improved by increasing the unit water content. However, an increase in the unit water content results in a decrease in concrete strength. Superplasticizers reduce the unit water content of concrete without causing a decline in its strength, while improving its workability. Thus, to achieve heating performance suitable for different applications of concrete, identifying the heating characteristics depending on the concrete mix is essential. In this study, concrete composites containing coarse aggregate and MWCNTs were produced. The aim of the study was to investigate the heating performance and characteristics of MWCNT concretes based on the coarse aggregate ratio, W/C ratio, and the presence or absence of superplasticizers.

2. Materials and Methods

2.1. Heat Generation Test Overview

In this study, tests were conducted to analyze the heating performance of concrete composites containing coarse aggregates. Table 1 lists the parameters considered for analyzing the heating performance. The test parameters included the coarse aggregate ratio, MWCNT content (wt.%), W/C ratio (%), and superplasticizer content (wt.%). The general weight ratio for mixing fine and coarse aggregates in concrete was 1:2:4, respectively. The coarse aggregate ratio was set at 40, 60, and 80% of the total aggregate weight, within a 20% range from the general weight ratio [27]. The MWCNT concentration was 0.25, 0.5, and 1.0 wt.% relative to the weight of cement [5–7]. The W/C ratio was set at 50, 55, and 60% based on KCS 14 20 10 [28]. The mixing ratio of the superplasticizer was approximately 2.0 wt.% of the cement weight, based on the range used in ultra-high-performance concrete [29].

Table 1. Test parameters.

Specimen Name	Coarse Aggregate Ratio (%)	MWCNT Content (wt.%)	W/C Ratio (%)	Superplasticizer (wt.%)
CA60-0.0-50-NSP	60	0.0	50	0.0
CA60-0.25-50-NSP	60	0.25	50	0.0
CA60-0.5-50-NSP	60	0.5	50	0.0
CA60-1.0-50-NSP	60	1.0	50	0.0
CA40-1.0-50-NSP	40	1.0	50	0.0
CA80-1.0-50-NSP	80	1.0	50	0.0
CA60-1.0-55-NSP	60	1.0	55	0.0
CA60-1.0-60-NSP	60	1.0	60	0.0
CA60-1.0-50-SP	60	1.0	50	1.0

The naming convention for the test specimens comprises the following. The first set of characters represents the mixing ratio of coarse aggregates, where “CA60” implies that the weight of coarse aggregate comprised 60% of the total aggregate weight. The second set of characters indicates the concentration of the incorporated MWCNTs, where “1.0” implies that the MWCNT content is 1.0 wt.% of the cement weight. The third set of characters represents the W/C ratio, where “50” represents a 50% W/C ratio. Finally, the fourth set of characters indicates the presence of superplasticizer, where “NSP” and “SP” signify no superplasticizer addition and superplasticizer addition, respectively. Therefore, CA60-1.0-50-SP represents an MWCNT concrete composite with a 60% coarse aggregate weight, 1.0 wt.% of MWCNT concentration, 50% W/C ratio, and added superplasticizer. Additionally, the reason for incorporating high-performance superplasticizer only in the CA60-1.0-50-SP was to compare and analyze the temperature difference of MWCNT concrete based on the presence or absence of superplasticizer.

The heating performance was analyzed by averaging the temperature change after excluding the maximum and minimum values following the heat generation test using five specimens prepared for each parameter. The microstructure of the MWCNT concrete composite was analyzed using a field emission scanning electron microscope (FE-SEM).

2.2. Specimen Preparation and Heat Generation Test Procedure

Figure 1 shows a schematic of the heat generation test specimen. The fabricated concrete had dimensions of 100 mm × 100 mm × 60 mm. The sand used in making the concrete followed the KSL ISO 679 standard, and ordinary Portland cement was used [30–32]. The coarse aggregate used followed the ASTM C 33 standard [33], with coarse aggregate particle diameters in the range of 4.75–9.5 mm. The MWCNTs had an average diameter and length of 9.5 nm and 1.5 μm, respectively, and were mixed with the specimens in an aqueous solution form to ensure dispersibility. The MWCNT aqueous solution was dispersed using ultrasound at 22 kHz in a polyacrylic acid copolymer for 8 h [34–37].

Table 2 lists the mix proportions of the specimens according to each parameter under consideration. MWCNTs, cement, fine aggregate, and coarse aggregate were appropriately mixed based on each parameter.

Figure 2 presents the production process followed to obtain the MWCNT concrete composite. First, the MWCNT aqueous solution, cement, and aggregate were measured to match the mix proportions of each set of specimens (Figure 2a). Cement and aggregate were then dry-mixed for 2 min to ensure material homogeneity, as shown in Figure 2b, followed by the mixing of the MWCNTs in an aqueous solution form and blending for 3 min (Figure 2c). Figure 2d depicts the process of pouring the mixed concrete into molds, which were tamped 30 times each for three rounds. Two stainless steel meshes were installed in the concrete at 40 mm intervals (Figure 2e). A thermocouple was inserted at a depth of 30 mm in the center of each specimen to measure the internal temperature during the heat

generation test, as shown in Figure 2f. To minimize the effects of moisture, the concrete was cured in dry conditions for 28 d after an initial 24 h curing period.

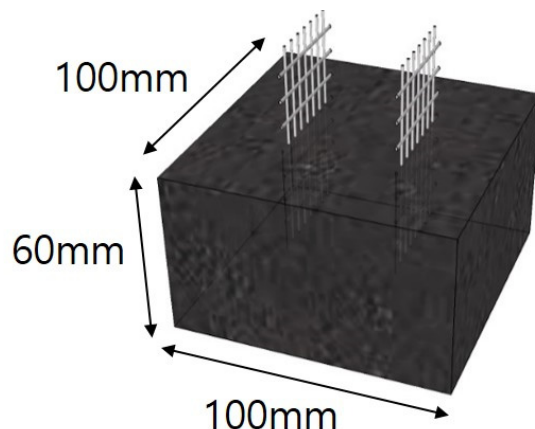


Figure 1. Heat generation test specimen.

Table 2. Mix proportion of specimens.

Specimen Name	MWCNT	Water	Cement	Fine Aggregate	Coarse Aggregate	Superplasticizer
CA60-0.0-50-NSP	0	150	300	300	450	0
CA60-0.25-50-NSP	0.75	150	300	300	300	0
CA60-0.5-50-NSP	1.5	150	300	300	300	0
CA60-1.0-50-NSP	3	150	300	300	300	0
CA40-1.0-50-NSP	3	150	300	408	272	0
CA80-1.0-50-NSP	3	150	300	170	680	0
CA60-1.0-55-NSP	2.85	156.75	285	300	450	0
CA60-1.0-60-NSP	2.7	162	270	300	450	0
CA60-1.0-50-SP	3	150	300	300	450	6

The heating performance of the concrete was tested by applying a constant voltage to each specimen. Figure 3 shows the heat generation test setup. Voltages of 10, 20, 30, and 60 V were applied using a DC power supply (EX-200, ODA Technologies., Incheon, Republic of Korea). The voltage was applied on an insulating rubber plate by connecting the (+) and (−) electrodes to the stainless steel mesh placed in the concrete for 60 min per specimen. The thermocouple installed during the fabrication process was connected to a data logger (TDS-303, Tokyo Sokki Kenkyujo Co., Ltd., Tokyo, Japan), to measure the internal temperature of the concrete, which rose due to the voltage. The surface temperature of the concrete was analyzed through thermal imaging when the temperature recorded by the data logger reached its peak.

FE-SEM was employed for analyzing the internal structure of the concrete composite. This procedure adheres to established guidelines, utilizing an accelerated electron beam emitted from a field emission electron gun (LEO SUPRA 55, ZEISS, Munich, Germany) to meticulously scan the specimen's surface. The detection of signals like secondary electrons, reflected electrons, and X-rays occurs during this scanning process. Subsequently, the generated magnified images are displayed or recorded on a cathode-ray tube, ensuring compliance with relevant regulations and protocols for analysis and interpretation. The sample preparation process for the FE-SEM analysis of the concrete composite was as follows. Initially, specimens sized at $1 \times 1 \times 1 \text{ cm}^3$ were selected and their surfaces delicately polished to ensure a uniform surface. Subsequently, the samples were securely affixed under vacuum conditions, followed by metal coating to enhance conductivity. Additionally, some samples underwent carbon coating on the surface to further ensure ample conductivity. These meticulously prepared samples were then employed for FE-SEM analysis.

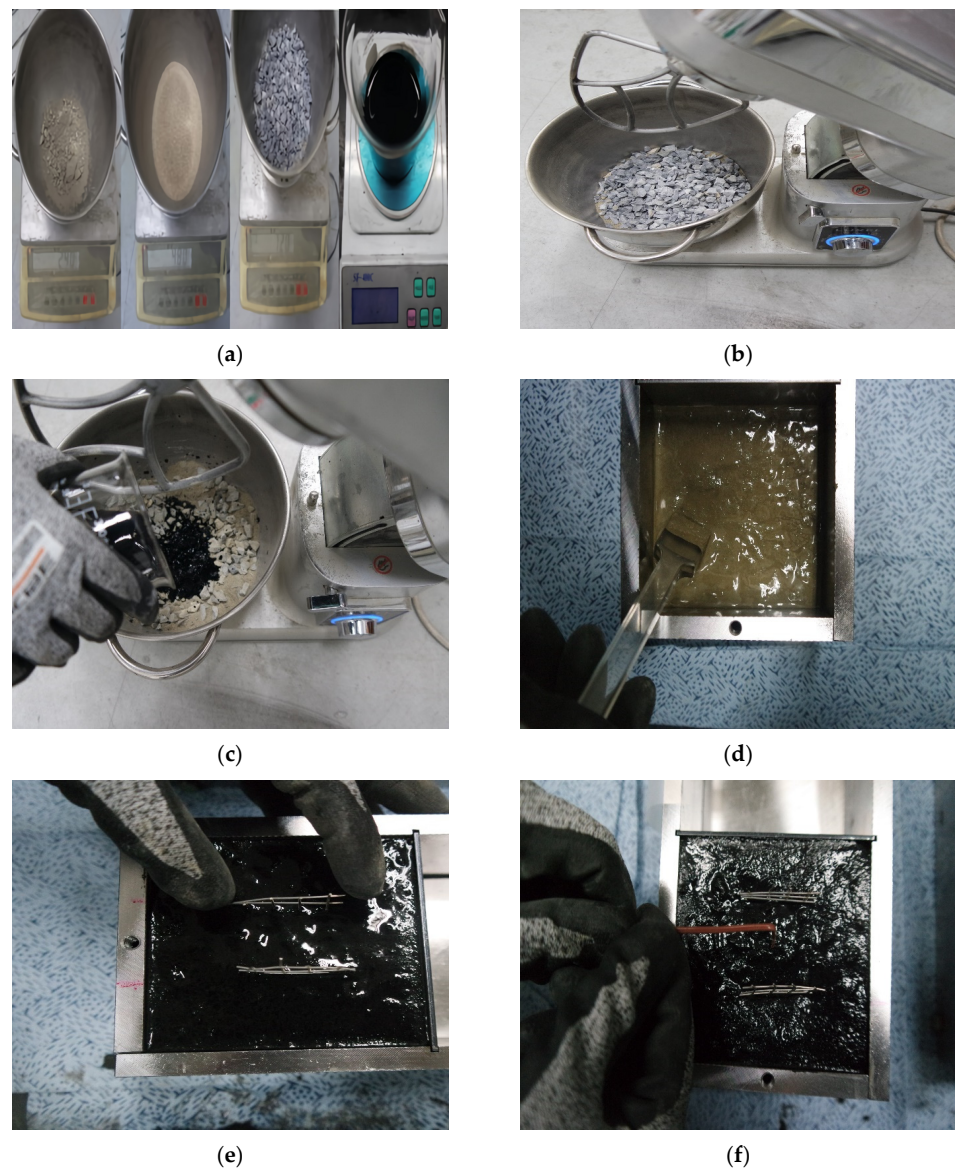


Figure 2. MWCNT concrete composite fabrication: (a) measuring materials; (b) dry-mixing (2 min); (c) MWCNT solution mixing (3 min); (d) tamping; (e) insert stainless steel mesh; and (f) insert thermocouple.

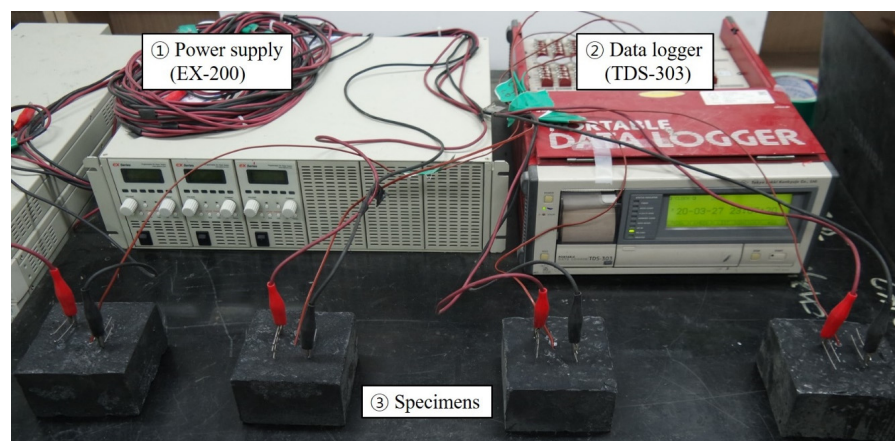


Figure 3. Test setup.

3. Results and Discussion

3.1. MWCNT Concentration

Figure 4 illustrates the heat generation test results of the concrete composite based on the concentration of MWCNT. The findings reveal distinct temperature variations concerning different applied voltages and MWCNT concentrations. At 10 V, specimens without MWCNTs exhibited a minimal temperature rise of 0.1 °C, while those infused with 0.25, 0.5, and 1.0 wt.% MWCNTs displayed gradual increases of 0.4, 0.9, and 1.6 °C, respectively.

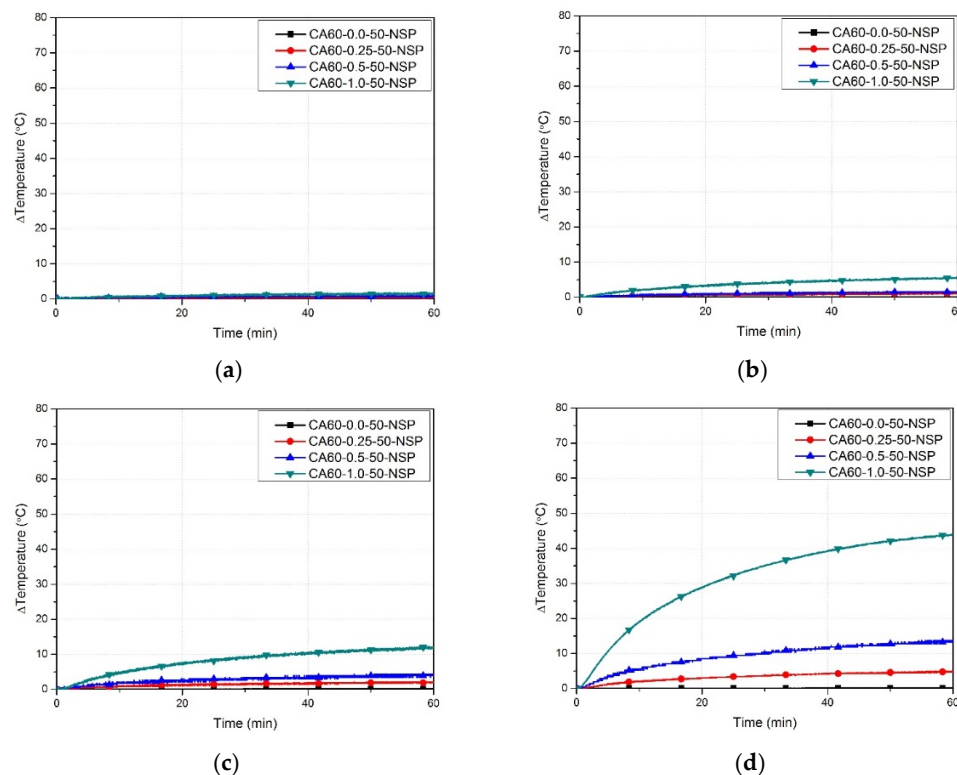


Figure 4. The heating performances of specimens by MWCNT concentration: (a) 10 V; (b) 20 V; (c) 30 V; and (d) 60 V.

Under 20 V, the recorded temperature increments in specimens with 0.0, 0.25, 0.5, and 1.0 wt.% MWCNTs were 0.1, 1.2, 1.7, and 5.3 °C, respectively. This escalating trend continued as higher voltages were applied. At 30 V, temperature escalations in specimens lacking MWCNTs reached 0.2 °C, contrasting significantly with those containing 0.25, 0.5, and 1.0 wt.% MWCNTs, which experienced rises of 2.1, 4.3, and 11.8 °C, respectively. Notably, the most prominent disparity was observed at 60 V, where temperatures rose by 0.2, 5.1, 14.2, and 43.8 °C in specimens containing 0.0, 0.25, 0.5, and 1.0 wt.% MWCNTs, respectively. These results underscore a significant correlation between MWCNT concentration and the resultant heat generation. The varying levels of temperature increase clearly delineate the pivotal role of MWCNT concentration in influencing the heating performance of the concrete composite.

The temperature increases for each specimen type based on the applied voltage are listed in Table 3. Specimens without MWCNTs show small temperature increases, which improve with increasing MWCNT concentration. The MWCNTs mixed into the concrete form a bridge network between the cement hydrates. When the mixed-in MWCNT concentration is increased, the formed bridge network increases, causing an increase in the current flowing through the concrete specimen. As the temperature increase is proportional to the electric current, it increases with the MWCNT concentration mixed into the concrete [8]. MWCNTs have high electrical conductivity. As the mixing concentration of MWCNTs increases, the electrical conductivity of MWCNT concrete increases. Multiple

MWCNT particles create a bridge network, which has the conductivity of concrete when supplying electricity.

Table 3. Results of heating performance according to the MWCNT concentration.

Specimen Name	Maximum Temperature Variation (°C)			
	10 V	20 V	30 V	60 V
CA60-0.0-50-NSP	0.1	0.1	0.2	0.2
CA60-0.25-50-NSP	0.4	1.2	2.1	5.1
CA60-0.5-50-NSP	0.9	1.7	4.3	14.2
CA60-1.0-50-NSP	1.6	5.3	11.8	43.8

For an applied voltage of 10 V, the thermal images of the concrete specimens mixed with different MWCNT concentrations are shown in Figure 5. At 10 V, the highest surface temperature of 20.2 °C was recorded for CA60-1.0-50-NSP, which was 6.3% higher than that of CA60-0.0-50-NSP. For an applied voltage of 60 V, the thermal images of the specimens mixed with different MWCNT concentrations are shown in Figure 6. At 60 V, the highest surface temperature of 66.4 °C was recorded for CA60-1.0-50-NSP (Figure 6d), which was 249.5% higher than that for CA60-0.0-50-NSP. The surface temperatures were consistently the highest for CA60-1.0-50-NSP for all applied voltages, similar to the heat generation test results based on the MWCNT concentration. Conversely, the surface temperatures of CA60-0.0-50-NSP without MWCNTs were similar to the ambient temperature. The surface temperatures were observed to increase with the MWCNT concentration when the same voltage was applied. Additionally, since the concrete was mixed with the aqueous solution of MWCNTs, heat diffused from the electrode areas connected to the voltage supply. Therefore, heat distribution was concluded to occur due to the property of current flowing through the shortest distance [38].

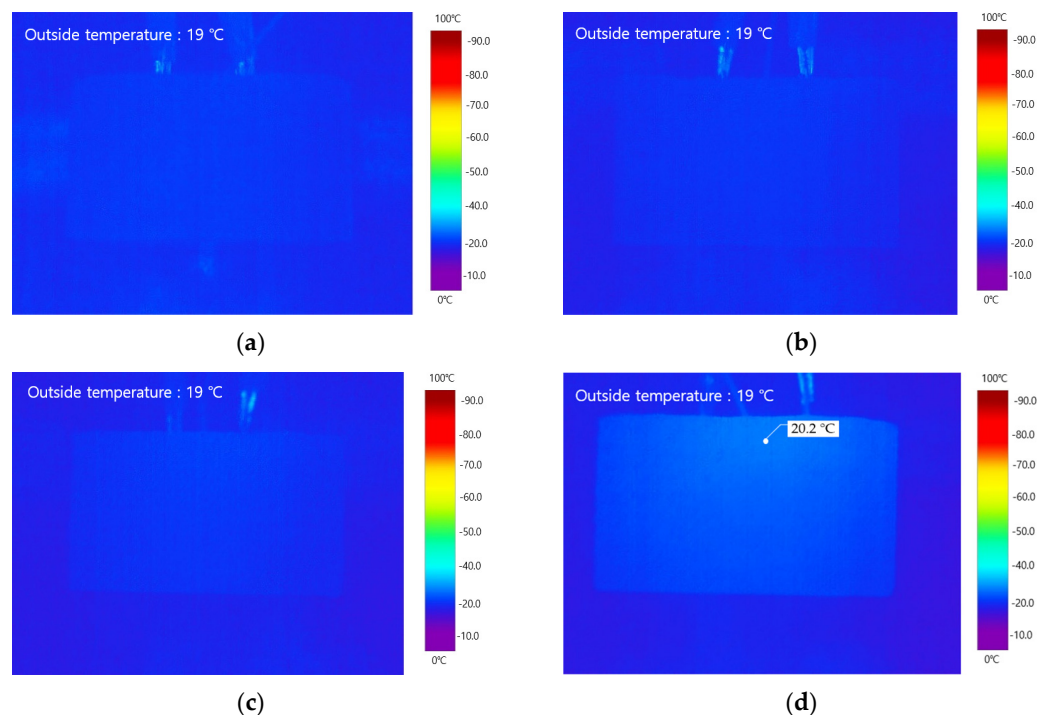


Figure 5. Thermal images of specimens according to MWCNT concentration (10 V): (a) 0.0 wt%; (b) 0.25 wt%; (c) 0.5 wt%; and (d) 1.0 wt%.

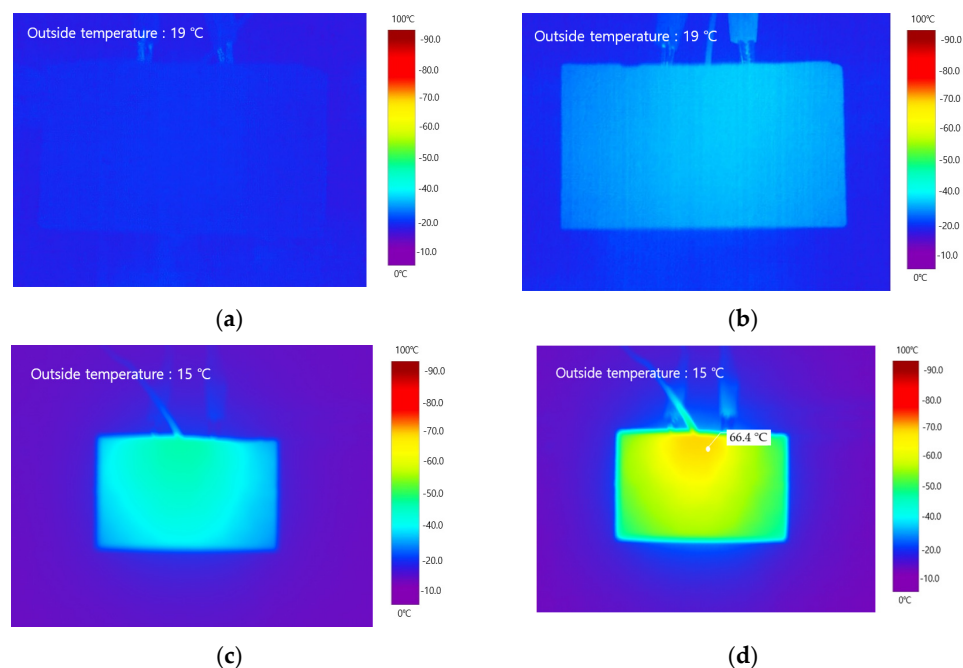


Figure 6. Thermal images of specimens according to MWCNT concentration (60 V): (a) 0.0 wt%; (b) 0.25 wt%; (c) 0.5 wt%; and (d) 1.0 wt%.

3.2. Coarse Aggregate Mixing Ratio

Figure 7 presents the heat generation test results obtained based on the mixing ratio of coarse aggregate. At 10 V, the temperature increases in the specimens with 40, 60, and 80% coarse aggregate mixing ratios were 2.1, 1.6, and 0.8 °C, respectively. Notably, even at 20 V, 30 V, and 60 V, the specimens with a 40% coarse aggregate mixing ratio exhibited the highest temperature rise, akin to those observed at 10 V. Upon the application of a 60 V voltage, the temperature variations in test specimens with coarse aggregate mixing ratios of 40%, 60%, and 80% were quantified at 56.1 °C, 43.8 °C, and 33.7 °C, respectively. These findings suggest that as the voltage increases, lower mixing ratios of coarse aggregate result in higher temperature rises. Additionally, test specimens containing more than 80% coarse aggregate showed temperature variations of up to 30 °C or more. This phenomenon allows us to conclude that heat generation is possible even in concrete specimens mixed with coarse aggregate.

The temperature increases of each specimen type at different applied voltages are listed in Table 4. The temperature increases improved as the mixing ratio of coarse aggregate decreased. The bridge networks were not formed by the MWCNTs within the aggregates. Conversely, for the same volume of the specimens, the greater the ratio of coarse aggregate, the less the space for forming a CNT network. Therefore, the temperature variation decreased due to poor dispersion and agglomeration of MWCNTs, which inhibited effective bridge network formation.

Table 4. Results of heating performance according to coarse aggregate ratio.

Specimen Name	Maximum Temperature Variation (°C)			
	10 V	20 V	30 V	60 V
CA40-1.0-50-NSP	2.1	6.4	14.6	56.1
CA60-1.0-50-NSP	1.6	5.3	11.8	43.8
CA80-1.0-50-NSP	0.8	4.1	8.3	33.7

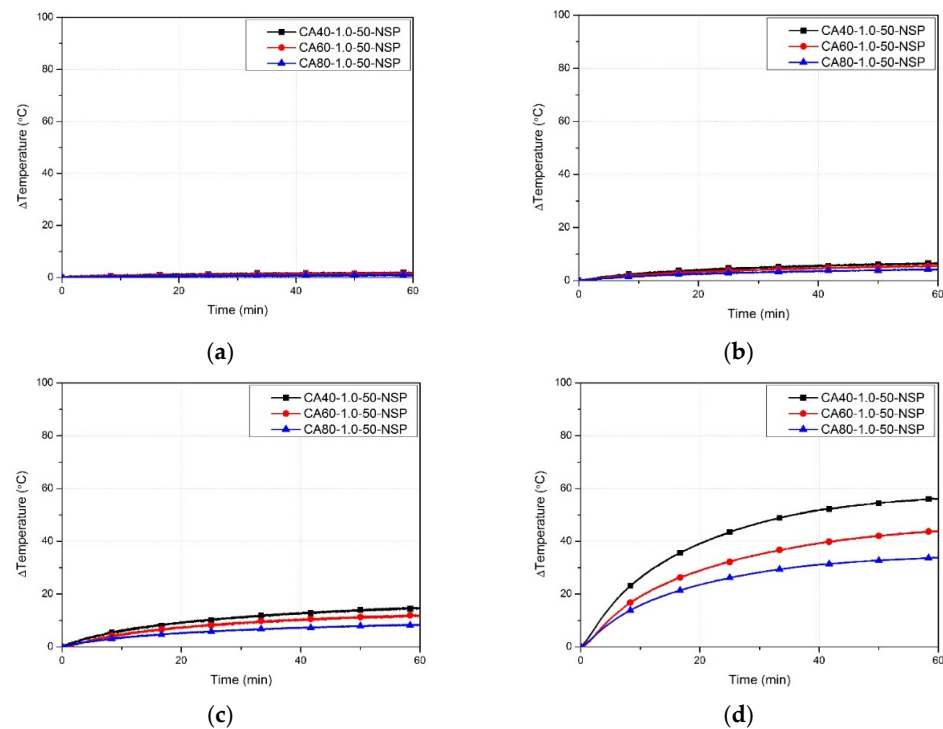


Figure 7. Temperature variations of specimens by coarse aggregate ratio: (a) 10 V; (b) 20 V; (c) 30 V; and (d) 60 V.

Figure 8 depicts the thermal images of the test specimens mixed with MWCNT based on the coarse aggregate mixing ratio. At 10 V, the highest surface temperature of 22.2 °C was recorded for CA40-1.0-50-NSP (Figure 8a), 14.4% higher than that for CA80-1.0-50-NSP (Figure 8b), which had the highest coarse aggregate mixing ratio. At 60 V, the thermal images of the specimens recorded based on the coarse aggregate mixing ratio are presented in Figure 8c,d. The highest surface temperature of 74.8 °C was recorded for CA40-1.0-50-NSP (Figure 8c), 25.5% higher than that for CA80-1.0-50-NSP. The surface temperature was the highest in CA40-1.0-50-NSP, similar to the heat generation test results; the surface temperature increased as the coarse aggregate mixing ratio decreased. The observed phenomenon was clearly distinguished through thermal images when the mixing ratio of coarse aggregate decreased.

3.3. W/C Ratio

Figure 9 showcases the heat generation test results based on the W/C ratio. At 10 V, the temperature increases in the specimens with 50, 55, and 60% W/C ratios were 1.6, 1.7, and 2.0 °C, respectively. At 20 V, the temperature increases in the specimens with 50, 55, and 60% W/C ratios were 1.6, 7.7, and 8.7 °C, respectively. At 30 V, the temperature increases in the specimens with 50, 55, and 60% W/C ratios were 11.8, 18.4, and 23.3 °C, respectively. At 60 V, the temperature increases in the specimens with 50, 55, and 60% W/C ratios were 43.8, 61.3, and 73.6 °C, respectively.

Table 5 lists the temperature increases of each specimen type at different applied voltages, based on the W/C ratio. The test results confirmed that the temperature increases in the specimens increased with their W/C ratio. When the MWCNT concentration in the concrete was maintained constantly, an equal weight of MWCNTs existed within all specimens; however, a higher W/C ratio reduced the weight ratio of MWCNTs to water, which lowered the MWCNT/water ratio, thereby enhancing the dispersibility of MWCNTs in the concrete [24]. Improved dispersibility of MWCNTs resulted in more evenly distributed bridge networks of MWCNT particles within the concrete [39]. The evenly

distributed bridge networks enhanced the heating performance of the concrete, leading to temperature increases rising with the W/C ratio.

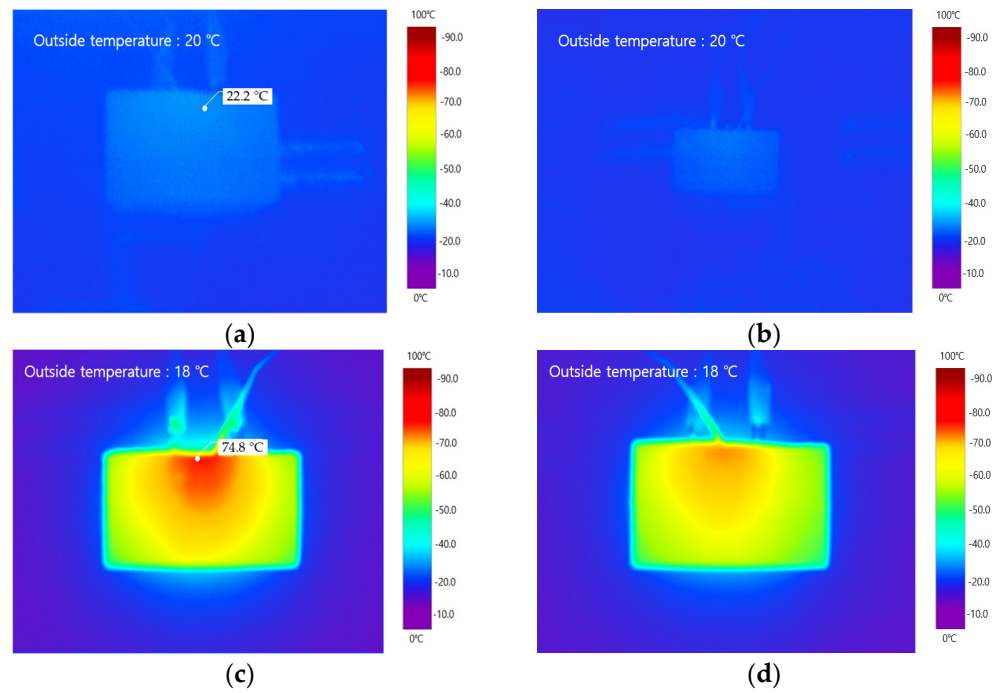


Figure 8. Thermal images of specimens according to coarse aggregate mixing ratio: (a) 40% (10 V); (b) 80% (10 V); (c) 40% (60 V); and (d) 80% (60 V).

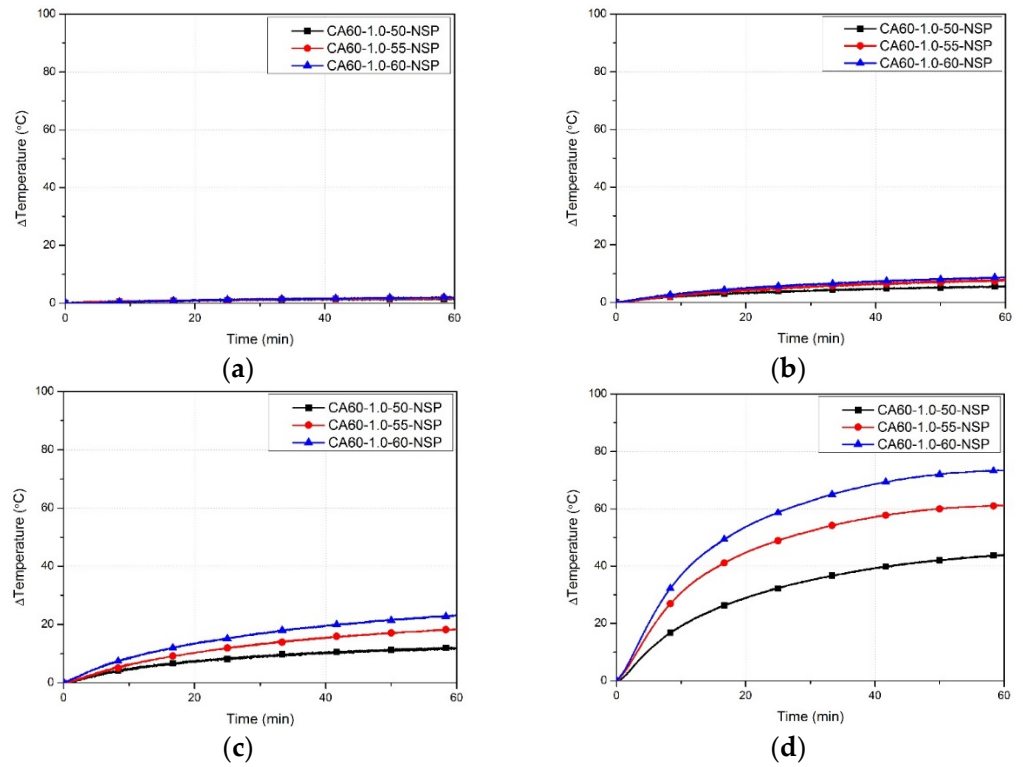


Figure 9. Temperature variations of specimens by W/C ratio: (a) 10 V; (b) 20 V; (c) 30 V; and (d) 60 V.

Table 5. Temperature increases according to W/C ratio.

Specimen Name	Maximum Temperature Variation (°C)			
	10 V	20 V	30 V	60 V
CA60-1.0-50-NSP	1.6	5.3	11.8	43.8
CA60-1.0-55-NSP	1.7	7.7	18.4	61.3
CA60-1.0-60-NSP	2.0	8.7	23.3	73.6

At 10 V, the thermal images of the concrete specimens based on the W/C ratio are shown in Figure 10. The highest surface temperature of 23.0 °C was recorded for CA60-1.0-60-NSP, which was 13.9% higher than that for CA60-1.0-50-NSP. At 60 V, the surface temperature of CA60-1.0-60-NSP was the highest at 86.8 °C (Figure 10d). The surface temperature of CA60-1.0-60-NSP was 30.7% higher than that of CA60-1.0-50-NSP.

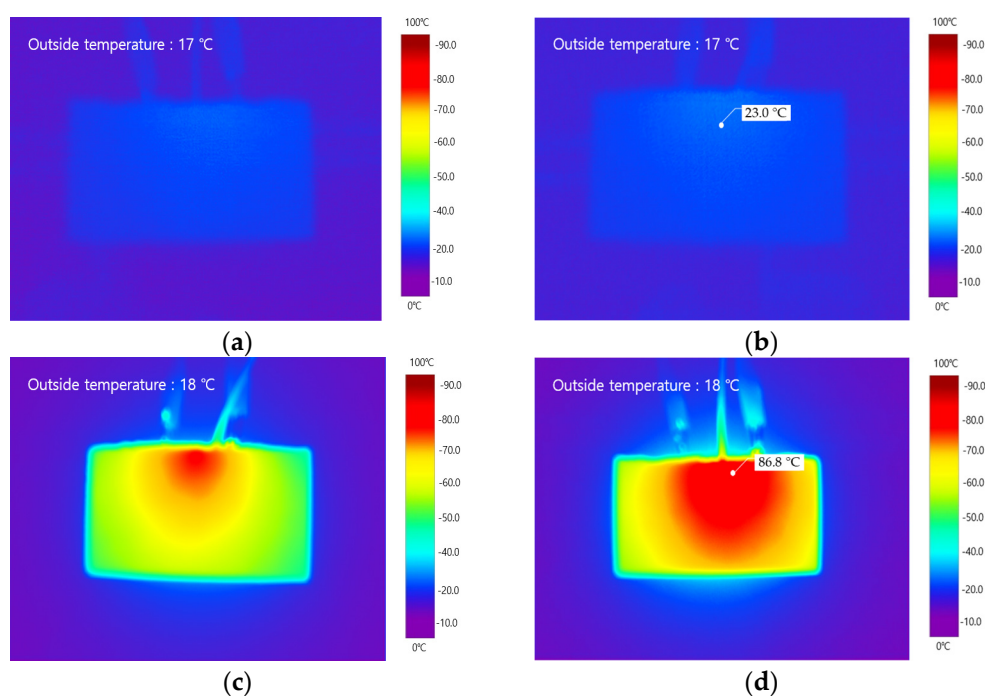


Figure 10. Thermal images of specimens according to W/C ratio: (a) 55% (10 V); (b) 60% (10 V); (c) 55% (60 V); and (d) 60% (60 V).

3.4. Presence or Absence of Superplasticizers

Figure 11 presents the heat generation test results obtained depending on the presence of a superplasticizer. CA60-1.0-50-NSP experienced a temperature drop due to a large temperature increase, and it broke down at an applied voltage of 30 V [22]. Therefore, a heating performance experiment based on the presence of superplasticizers was conducted with applied voltages limited to 10, 20, and 30 V. At 10 V, the temperature increases in the specimens without and with superplasticizer were 1.6 and 5 °C, respectively (Figure 11a). At 20 V, the temperature increases in the specimens without and with superplasticizer were 5.3 and 16.9 °C, respectively (Figure 11b). At 30 V, the temperature increases in the specimens without and with the superplasticizer were 11.8 and 48.6 °C, respectively (Figure 11c).

Table 6 lists the temperature differences for each specimen type at different applied voltages, based on the presence or not of a superplasticizer. The test results indicated an increase in heat generation with the addition of a superplasticizer. The superplasticizer enhanced the dispersibility of the MWCNTs [26], causing an even formation of the MWCNT particles within the concrete. As CNT particles were more evenly dispersed within the

concrete, the heating performance of the MWCNT concrete improved when the superplasticizer was added. At 10 V, the thermal images of the concrete specimens based on the presence of superplasticizer are presented in Figure 12a. The highest surface temperature recorded was 24.1 °C, which is 19.3% higher than that for the specimens with no added superplasticizer. At 30 V, the thermal images of the specimens based on the presence of a superplasticizer are shown in Figure 12b. The highest surface temperature recorded was 39.3 °C.

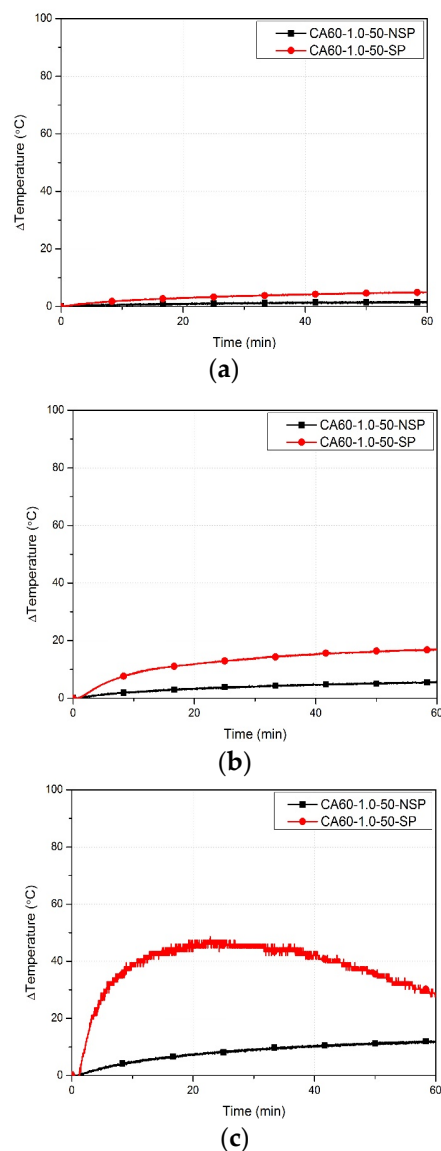


Figure 11. Temperature variations of specimens with/without superplasticizer: (a) 10 V; (b) 20 V; and (c) 30 V.

Figure 13 displays the FE-SEM images representing specimens containing MWCNTs. These images were generated for CA60-0.0-50-NSP and CA60-1.0-50-NSP, where MWCNTs are highlighted in red. In Figure 13a, the FE-SEM image of CA60-0.0-50-NSP reveals the absence of MWCNTs. Consequently, only hydrates are observable in the image. Contrarily, Figure 13b illustrates the FE-SEM image of CA60-1.0-50-NSP, demonstrating a notable presence of MWCNTs. This specimen showcases the formation of a remarkable network of MWCNT bridges. These bridges visibly interconnect MWCNT particles with the hydrates, suggesting a significant contribution of the nanotubes to the structural arrangement within the composite material. Unlike CA60-0.0-50-NSP, CA60-1.0-50-NSP displays the formation

of an intricate MWCNT bridge network. This network, comprised of interconnected nanotubes and hydrates, potentially enhances the composite material's mechanical and structural properties, indicating the influential role of MWCNTs in modifying the material's characteristics.

Table 6. Results of heating performance according to presence of superplasticizer.

Specimen Name	Maximum Temperature Variation (°C)		
	10 V	20 V	30 V
CA60-1.0-50-NSP	1.6	5.3	11.8
CA60-1.0-50-SP	5.0	16.9	48.6

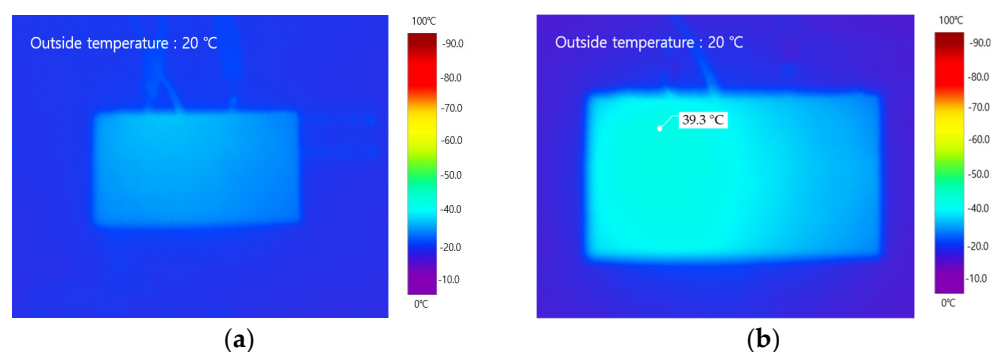


Figure 12. Thermal images of specimens with superplasticizers: (a) 10 V and (b) 30 V.

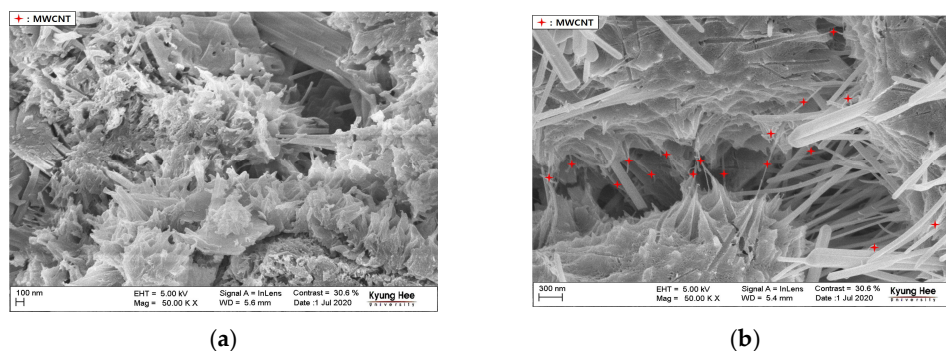


Figure 13. FE-SEM images: (a) CA60-0.0-50-NSP and (b) CA60-1.0-50-NSP.

4. Conclusions

In this study, concrete specimens were mixed with MWCNTs, which possess excellent thermal properties, and tests on heating performance were conducted for microstructure analyses. Based on the experimental results, the following conclusions were drawn:

1. The heating performance of the concrete improved as the MWCNT concentration increased. An increased MWCNT concentration resulted in more MWCNT bridge networks forming within the concrete; these bridge networks served as an electron transport pathway, thereby imparting conductivity to the concrete.
2. The heating performance of the concrete improved when the coarse aggregate mixing ratio was decreased. A higher mixing ratio of coarse aggregate reduced the space available for MWCNTs to disperse within the specimen, which caused MWCNT agglomeration and the degradation of MWCNT bridge network formation, resulting in weaker heating performance.
3. The heating performance of the concrete improved with an increase in the W/C ratio. A high W/C ratio aided in the even dispersion of MWCNTs within the concrete. As the W/C ratio increased, the phenomenon of MWCNT agglomeration decreased,

and the even distribution of CNT particles enhanced the electron mobility, thereby improving the heating performance.

4. The heating performance of the concrete improved when a superplasticizer (a typical admixture) was added, as it enhanced the dispersibility of the MWCNT particles. Similar to the results obtained for a high W/C ratio, adding a superplasticizer induced an even distribution of CNT particles and improved the heating performance of the concrete.
5. FE-SEM imaging confirmed the formation of MWCNT bridge networks connecting the concrete hydrates. The formed MWCNT bridge network acted as an electron transport path and improved the conductivity of the concrete.
6. Another promising area for future work is an analysis of how the density of concrete influences thermal characteristics when modified with nanomaterials. This could involve exploring the applicability of such modifications to different types of concrete, such as cellular concrete, lightweight concrete, or denser concrete. By addressing these aspects, a more comprehensive understanding of the broader implications of nanomaterial modifications on concrete properties can be achieved. Furthermore, additional research is planned to verify the applicability of MWCNT concrete to heat generation by applying it to the field.

Therefore, by mixing MWCNT aqueous solutions into concrete and using an appropriate W/C ratio and superplasticizer, the concrete can be used as a new construction material with strong heating performance.

Author Contributions: Conceptualization, H.Y. and W.C.; methodology, D.K.; formal analysis, S.K.; investigation, H.Y. and D.K.; data curation, H.Y. and W.C.; writing—original draft preparation, S.K.; project administration. All authors have read and agreed to the published version of the manuscript.

Funding: This research was supported by “Regional Innovation Strategy (RIS)” through the National Research Foundation of Korea (NRF) funded by the Ministry of Education (MOE) (2021RIS-002).

Data Availability Statement: The data presented in this study are available in the article.

Conflicts of Interest: The authors declare no conflict of interest.

References

1. Li, H.; Zhang, Q.; Xiao, H. Self-deicing road system with a CNFP high-efficiency thermal source and MWCNT/cement-based high-thermal conductive composites. *Cold Reg. Sci. Technol.* **2013**, *86*, 22–35. [\[CrossRef\]](#)
2. Gomis, J.; Galao, O.; Gomis, V.; Zornoza, E.; Garcés, P. Self-heating and deicing conductive cement. Experimental study and modeling. *Constr. Build. Mater.* **2015**, *75*, 442–449. [\[CrossRef\]](#)
3. Kim, G.M.; Naeem, F.; Kim, H.K.; Lee, H.K. Heating and heat-dependent mechanical characteristics of CNT-embedded cementitious composites. *Compos. Struct.* **2016**, *136*, 162–170. [\[CrossRef\]](#)
4. Kim, G.M.; Yang, B.J.; Ryu, G.U.; Lee, H.K. The electrically conductive carbon nanotube (CNT)/cement composites for accelerated curing and thermal cracking reduction. *Compos. Struct.* **2016**, *158*, 20–29. [\[CrossRef\]](#)
5. Lee, H.; Kang, D.; Song, Y.M.; Chung, W. Heating experiment of CNT cementitious composites with single-walled and multiwalled carbon nanotubes. *J. Nanomater.* **2017**, *2017*, 3691509. [\[CrossRef\]](#)
6. Lee, H.; Song, Y.M.; Loh, K.J.; Chung, W. Thermal response characterization and comparison of carbon nanotube-enhanced cementitious composites. *Compos. Struct.* **2018**, *202*, 1042–1050. [\[CrossRef\]](#)
7. Lee, H.; Park, S.; Cho, S.; Chung, W. Correlation analysis of heating performance and electrical energy of multi-walled carbon nanotubes cementitious composites at sub-zero temperatures. *Compos. Struct.* **2020**, *238*, 111977. [\[CrossRef\]](#)
8. Konsta-Gdoutos, M.S.; Metaxa, Z.S.; Shah, S.P. Highly dispersed carbon nanotube reinforced cement based materials. *Cem. Concr. Res.* **2010**, *40*, 1052–1059. [\[CrossRef\]](#)
9. Liew, K.M.; Kai, M.F.; Zhang, L.W. Carbon nanotube reinforced cementitious composites: An overview. *Compos. Part A Appl. Sci. Manuf.* **2016**, *91*, 301–323. [\[CrossRef\]](#)
10. Li, G.Y.; Wang, P.M.; Zhao, X. Pressure-sensitive properties and microstructure of carbon nanotube reinforced cement composites. *Cem. Concr. Compos.* **2007**, *29*, 377–382. [\[CrossRef\]](#)
11. Zou, B.; Chen, S.J.; Korayem, A.H.; Collins, F.; Wang, C.M.; Duan, W.H. Effect of ultrasonication energy on engineering properties of carbon nanotube reinforced cement pastes. *Carbon* **2015**, *85*, 212–220. [\[CrossRef\]](#)

12. Sindu, B.S.; Sasmal, S. Properties of carbon nanotube reinforced cement composite synthesized using different types of surfactants. *Constr. Build. Mater.* **2017**, *155*, 389–399. [[CrossRef](#)]
13. Dong, W.; Li, W.; Wang, K.; Han, B.; Sheng, D.; Shah, S.P. Investigation on physicochemical and piezoresistive properties of smart MWCNT/cementitious composite exposed to elevated temperatures. *Cem. Concr. Compos.* **2020**, *112*, 103675. [[CrossRef](#)]
14. Jang, D.; Yoon, H.N.; Seo, J.; Yang, B. Effects of exposure temperature on the piezoresistive sensing performances of MWCNT-embedded cementitious sensor. *J. Build. Eng.* **2022**, *47*, 103816. [[CrossRef](#)]
15. Nalon, G.H.; Ribeiro, J.C.L.; Pedroti, L.G.; de Araújo, E.N.D.; de Carvalho, J.M.F.; de Lima, G.E.S.; de Moura Guimarães, L. Residual piezoresistive properties of mortars containing carbon nanomaterials exposed to high temperatures. *Cem. Concr. Compos.* **2021**, *121*, 104104. [[CrossRef](#)]
16. Won, J.P.; Kim, C.K.; Lee, S.J.; Lee, J.H.; Kim, R.W. Thermal characteristics of a conductive cement-based composite for a snow-melting heated pavement system. *Compos. Struct.* **2014**, *118*, 106–111. [[CrossRef](#)]
17. Sassani, A.; Ceylan, H.; Kim, S.; Arabzadeh, A.; Taylor, P.C.; Gopalakrishnan, K. Development of carbon fiber-modified electrically conductive concrete for implementation in Des Moines International Airport. *Case Stud. Constr. Mater.* **2018**, *8*, 277–291. [[CrossRef](#)]
18. Metaxa, Z.S.; Boutsoukou, S.; Amenta, M.; Favvas, E.P.; Kourkoulis, S.K.; Alexopoulos, N.D. Dispersion of Multi-Walled Carbon Nanotubes into White Cement Mortars: The Effect of Concentration and Surfactants. *Nanomaterials* **2022**, *12*, 1031. [[CrossRef](#)]
19. Sharma, S.; Kothiyal, N.C. Facile growth of carbon nanotubes coated with carbon nanoparticles: A potential low-cost hybrid nanoadditive for improved mechanical, electrical, microstructural and crystalline properties of cement mortar matrix. *Constr. Build. Mater.* **2016**, *123*, 829–846. [[CrossRef](#)]
20. Dalla, P.T.; Tragazikis, I.K.; Trakakis, G.; Galiotis, C.; Dassios, K.G.; Matikas, T.E. Multifunctional cement mortars enhanced with graphene nanoplatelets and carbon nanotubes. *Sensors* **2021**, *21*, 933. [[CrossRef](#)]
21. Kim, G.M.; Yoon, H.N.; Lee, H.K. Autogenous shrinkage and electrical characteristics of cement pastes and mortars with carbon nanotube and carbon fiber. *Constr. Build. Mater.* **2018**, *177*, 428–435. [[CrossRef](#)]
22. Kaur, R.; Kothiyal, N.C.; Arora, H. Studies on combined effect of superplasticizer modified graphene oxide and carbon nanotubes on the physico-mechanical strength and electrical resistivity of fly ash blended cement mortar. *J. Build. Eng.* **2020**, *30*, 101304. [[CrossRef](#)]
23. Han, B.; Yu, X.; Kwon, E. A self-sensing carbon nanotube/cement composite for traffic monitoring. *Nanotechnology* **2009**, *20*, 445501. [[CrossRef](#)] [[PubMed](#)]
24. Han, B.; Yu, X.; Kwon, E.; Ou, J. Effects of CNT concentration level and water/cement ratio on the piezoresistivity of CNT/cement composites. *J. Compos. Mater.* **2012**, *46*, 19–25. [[CrossRef](#)]
25. Jang, S.H.; Hochstein, D.P.; Kawashima, S.; Yin, H. Experiments and micromechanical modeling of electrical conductivity of carbon nanotube/cement composites with moisture. *Cem. Concr. Compos.* **2017**, *77*, 49–59. [[CrossRef](#)]
26. Park, H.M.; Kim, G.M.; Lee, S.Y.; Jeon, H.; Kim, S.Y.; Kim, M.; Yang, B.J. Electrical resistivity reduction with pitch-based carbon fiber into multi-walled carbon nanotube (MWCNT)-embedded cement composites. *Constr. Build. Mater.* **2018**, *165*, 484–493. [[CrossRef](#)]
27. Udoye, F.F.; Iron, U.H.; Odum, O.O. Strength performance of laterized concrete. *Constr. Build. Mater.* **2006**, *20*, 1057–1062. [[CrossRef](#)]
28. *KCS 14 20 10*; Concrete, Korean Construction Specification. Korean Standards Association: Seoul, Republic of Korea, 2016.
29. Shi, C.; Wu, Z.; Xiao, J.; Wang, D.; Huang, Z.; Fang, Z. A review on ultra high performance concrete: Part I. Raw materials and mixture design. *Constr. Build. Mater.* **2015**, *101*, 741–751. [[CrossRef](#)]
30. *ASTM C 109*; Standard Test Method for Compressive Strength of Hydraulic Cement Mortars (Using 2-in, or [50-mm] Cube Specimens). ASTM International: West Conshohocken, PA, USA, 2016.
31. *KS L ISO 679*; Methods of Testing Cements—Determination of Strength. Korean Agency for Technology and Standards (KATs): Eumseong, Republic of Korea, 2006.
32. *ISO 679*; Cement—Test Methods—Determination of Strength. ISO (International Organization for Standardization): Geneva, Switzerland, 2009.
33. *ASTM C 33*; Standard Specification for Concrete Aggregates. In Annual Book of ASTM Standards. American Society for Testing and Materials: West Conshohocken, PA, USA, 1997.
34. Lee, H.; Jeong, S.; Park, S.; Chung, W. Enhanced mechanical and heating performance of multi-walled carbon nanotube-cement composites fabricated using different mixing methods. *Compos. Struct.* **2019**, *225*, 111072. [[CrossRef](#)]
35. Wang, B.; Han, Y.; Liu, S. Effect of highly dispersed carbon nanotubes on the flexural toughness of cement-based composites. *Constr. Build. Mater.* **2013**, *46*, 8–12. [[CrossRef](#)]
36. Kim, G.M.; Yang, B.J.; Cho, K.J.; Kim, E.M.; Lee, H.K. Influences of CNT dispersion and pore characteristics on the electrical performance of cementitious composites. *Compos. Struct.* **2017**, *164*, 32–42. [[CrossRef](#)]
37. Hu, Y.; Luo, D.; Li, P.; Li, Q.; Sun, G. Fracture toughness enhancement of cement paste with multi-walled carbon nanotubes. *Constr. Build. Mater.* **2014**, *70*, 332–338. [[CrossRef](#)]

38. Lee, H.; Yu, W.; Loh, K.J.; Chung, W. Self-heating and electrical performance of carbon nanotube-enhanced cement composites. *Constr. Build. Mater.* **2020**, *250*, 118838. [[CrossRef](#)]
39. Kim, H.K.; Nam, I.W.; Lee, H.K. Enhanced effect of carbon nanotube on mechanical and electrical properties of cement composites by incorporation of silica fume. *Compos. Struct.* **2014**, *107*, 60–69. [[CrossRef](#)]

Disclaimer/Publisher’s Note: The statements, opinions and data contained in all publications are solely those of the individual author(s) and contributor(s) and not of MDPI and/or the editor(s). MDPI and/or the editor(s) disclaim responsibility for any injury to people or property resulting from any ideas, methods, instructions or products referred to in the content.